*Journal of Zhejiang University-SCIENCE B (Biomedicine & Biotechnology) in press*
www.jzus.zju.edu.cn; www.springer.com/journal/11585
E-mail: jzus_b@zju.edu.cn

**Research Article**

https://doi.org/10.1631/jzus.B2500269

# Single-cell profiling of liver in offspring with intrauterine hyperglycemia reveals acute-phase response deficiency

Jiahang MO[1*], Jing YAN[1*], Yi CHENG[2*], Kaixuan DONG[3], Tianyou WANG[4], Jie LI[1], Meijun PAN[1], Guolian DING[1,5], Hong ZHU[1,5✉], Hefeng HUANG[1,5,6,7✉]

[1]*Obstetrics and Gynecology Hospital, Institute of Reproduction and Development, Fudan University, Shanghai 200090, China*
[2] *The First Affiliated Hospital, Zhejiang University School of Medicine, Hangzhou 310006, China*
[3] *Department of Obstetrics and Gynecology, Peking Union Medical College Hospital, Chinese Academy of Medical Sciences and Peking Union Medical College, Beijing 100005, China*
[4] *Department of Gynecology Oncology, Obstetrics and Gynecology Hospital, Fudan University, Shanghai 200090, China*
[5] *Shanghai Key Laboratory of Reproduction and Development, Shanghai 200032, China*
[6] *Key Laboratory of Reproductive Genetics (Ministry of Education), Department of Reproductive Endocrinology, Women's Hospital, Zhejiang University School of Medicine, Hangzhou 310006, China;*
[7] *Research Units of Embryo Original Diseases, Chinese Academy of Medical Sciences (No. 2019RU056), Shanghai 200032, China.*



**Abstract: Background:** Gestational diabetes mellitus (GDM) has long-term effects on offspring health. In the development of this chronic disease, inflammatory profiles play important roles. However, the assessment of GDM fetuses for their inflammatory status has been limited. Thus, single-cell RNA sequencing (scRNA-seq) is urgently needed to delineate the inflammatory characteristics of offspring with intrauterine hyperglycemia (IHG). **Methods:** A mouse IHG model was induced by streptozotocin (STZ). Liver samples of offspring at the fetal and adult periods were collected for scRNA-seq analysis and further experiments. CytoTRACE and Monocle were used for the developmental analysis of fetal liver after dimension reduction and clustering. The CellChat algorithm was applied for the cellular interaction analysis of adult livers. A lipopolysaccharide (LPS)-induced sepsis model was built in adult offspring to evaluate the immune response. Subsequently, primary cell flow cytometry (FCM) of the bone marrow (BM) and liver was performed for myeloid lineage detection. Finally, the transcriptional and translational levels of acute-phase response cytokines were quantified. **Results:** Our study has mapped the single-cell profile of livers in offspring with IHG. Myeloid polarization was identified, accompanied by the developmental retardation of multiple cell lineages in IHG offspring. In adults, myeloid polarization was restored to some extent, while the proinflammatory potential of these myeloid cells seemed to be deeply molded. Adult offspring with IHG also showed deficiency in acute-phase response in the LPS-induced sepsis model. **Conclusions:** The single-cell profile of livers from offspring with IHG highlighted the comprehensive inflammatory status of the myeloid lineage and hinted acute-phase response deficiency in sepsis.

**Key words:** Intrauterine hyperglycemia (IHG); Single-cell RNA sequencing (sc-RNA seq); Liver; Myeloid cell; Inflammation; Acute-phase response

## 1 Introduction

Gestational diabetes mellitus (GDM), most commonly causing intrauterine hyperglycemia (IHG), is a major complication of pregnancy (Mcintyre et al., 2019). Current studies have paid more attention to the

✉ Hong ZHU, Zhuhong-hope@163.com
✉ Hefeng HUANG, huanghefg@hotmail.com
*The three authors contributed equally to this work
Hefeng HUANG, https://orcid.org/0000-0002-0195-985X

Received May 20, 2025; Revision accepted Sept. 22, 2025;
Crosschecked xxx. xx, 20xx; Published online xxx. xx, 20xx

long-term influence of GDM on offspring (Bianco and Josefson, 2019). In addition to the metabolic disorder (Zhu et al., 2019; Jiang et al., 2022; Fang et al., 2023), researchers have also focused on the susceptibility to cognitive dysfunction (Zou et al., 2021; Luo et al., 2022), atherosclerosis (Govindarajah et al., 2024), and nonalcoholic fatty liver disease (Foo et al., 2024) in offspring with GDM mothers. The systematic and organic inflammatory microenvironment is considered to be one of the essential factors contributing to the poor health state of GDM offspring (De Mendonca et al., 2022; Pascoe et al., 2022). Dong et al. reported that IHG exposure was associated with increased inflammation in the liver of adult male offspring, which was mediated by the activation of Janus Kinase 2 (JAK2) and the signal transducer and activator of transcription 3 (STAT3) signaling (Dong et al., 2021). Govindarajah, et al. (2024) combined atherosclerosis-prone *Apoe*-KO mice with the streptozotocin (STZ) protocol and showed that diabetic pregnancy promoted atherosclerosis development in adult offspring via more severe inflammatory infiltration. Thus, understanding the inflammatory status in offspring with IHG is essential for adult disease susceptibility.

Multiple sequencing methods, such as transcriptome sequencing, whole genome bisulfite sequencing (WGBS) (Ding et al., 2012; Pinney et al., 2020), and chromatin immunoprecipitation sequencing (ChIP-seq), have been performed in studies on GDM offspring (Yan et al., 2024). Based on single-cell RNA sequencing (scRNA-seq), Yang et al. generated a comprehensive transcriptomic profile of cellular signatures in the human placenta with GDM and observed a trend towards M2 polarization in samples (Yang et al., 2021). Another study using scRNA-seq for human GDM cord blood identified a group of CXCL8+ IL1β+ monocytes. These neonatal monocytes were characterized by increased phagocytic and adhesion ability and shared the transcriptional traits with plaque myeloid cells (Yin et al., 2024). Although the above studies explored the inflammatory status of neonatal offspring with GDM mothers based on scRNA-seq, their conclusions do not seem to be fully consistent because of the discrepancy of samples. scRNA-seq of fetal appendages merely reflected the immediate state of these inflammatory cells exposed to IHG, whereas they lacked exploring long-term disease susceptibility in adult offspring with GDM mothers.

In this study, we established an IHG mouse model and performed scRNA-seq of fetal (E18.5) and adult (eight weeks) male offspring livers. The single-cell profiles and developmental state of offspring livers were analyzed during the fetal period, when the liver serves as a temporary hematopoietic organ. Subsequent analysis of adult offspring liver traced the inflammatory components derived from fetal liver. Overall, abnormal patterns of myeloid lineage in livers of offspring with IHG mothers were confirmed, and their deficiency in acute-phase response was verified in a lipopolysaccharide (LPS)-induced sepsis model.

## 2 Materials and methods

### 2.1 Animal care

All procedures for animal experiments were conducted in accordance with the Guide for the Care and Use of Laboratory Animals at Shanghai Model Organisms (Shanghai, China) (approval ID for the animal IACUC protocol: 2019-0026). Male and female C57BL/6J mice were purchased from Shanghai Model Organisms. All mice were housed under a light: dark cycle of 12 h:12 h and a temperature of (21±1) °C, with food and water provided *ad libitum*.

### 2.2 Intrauterine hyperglycemia model

Twelve adult male mice aged 14 to 16 weeks were mated with 8-week-old virgin female mice at a 1:2 ratio to obtain offspring. After mating, female mice with vaginal plugs were considered as pregnant for 0.5 d (E0.5) and singly housed for the completion of gestation. Pregnant mice were randomly assigned to Ctrl group and IHG group. Mice in the IHG group were injected intraperitoneally with STZ (150 mg/kg; Sigma-Aldrich, St. Louis, Missouri, USA), and Ctrl mice were injected intraperitoneally with an equal amount of sodium citrate buffer (Solarbio, Beijing, China). IHG mice with random blood glucose >16.7 mmol/L were considered as successful establishment of the model (Zhu, et al., 2019). F1 offspring from Ctrl and IHG groups were

foster-fed by normal female mice. Both Ctrl-F1 and IHG-F1 offspring were weaned at three weeks of age.

### 2.3 Sepsis model

Adult offspring at the age of 8 weeks used for LPS-induced (Sigma-Aldrich) sepsis model building. With reference to previous literature (Sun et al., 2022), three doses of 0.1, 1.0, and 10.0 mg/kg LPS were set to evaluate the liver response. Significant infiltration of inflammatory cells was found in the liver at 1.0 mg/kg LPS, to which the mice were somewhat tolerant. In the formal experiment, Ctrl and IHG F1 offspring mice were fasted for 14 h and then intraperitoneally injected with LPS (1.0 mg/kg). Twelve hours after LPS injection, mice with typical symptoms of sepsis (diarrhea, eyelid pus, and energy loss) were sacrificed for subsequent experiments.

### 2.4 Single-cell RNA sequencing (scRNA-seq)

Fetal male offspring at E18.5 were obtained by Caesarean section, and adult male offspring at eight weeks were sacrificed for liver scRNA-seq. Samples were pooled from three pregnant mice. Fresh liver specimens were immediately preserved in a special storage solution and transported to Oebiotech (Shanghai, China) at low temperature for scRNA-seq. The 10× Genomics platform used is based on microfluidics technology. Cells and beads with cell barcode were wrapped in the droplets, and the droplets containing cells were collected. Cells were lysed in the droplets, and their messenger RNAs (mRNAs) were connected with the barcode to form single-cell gel bead-in-emulsions (GEMs). The reverse transcription reaction was performed in the droplets. Subsequently, the complementary DNA (cDNA) library was constructed, and the sample index on library sequence was used to distinguish the sample source of target sequence.

### 2.5 scRNA-seq analysis

The Cell Ranger software (version 5.0.0) affiliated to 10× Genomics was used to demultiplex cellular barcodes, map reads to the genome and transcriptome using the Spliced Transcripts Alignment to a Reference (STAR) aligner, and down-sample reads as required to generate normalized aggregate data across samples, producing a matrix of gene counts versus cells. To process the unique molecular identifier (UMI) count matrix, the R package 'Seurat' (version 4.3.0) was used (Butler et al., 2018). Quality control was considered complete after discarding cells with high mitochondrial ratio (>10% of the counts belonged to mitochondrial genes) and doublets (DoubletFinder package; 2.3.0) (Mcginnis et al., 2019). Library size normalization was performed with the NormalizeData function in Seurat to obtain the normalized count. To remove the batch effects in single-cell RNA-sequencing data, the mutual nearest neighbors (MNN) presented by Haghverdi et al. (2018)was performed with the R package 'batchelor'. Graph-based clustering was performed to cluster cells according to their gene expression profile using the FindClusters function in Seurat.

Cells were visualized using a 2-dimensional Uniform Manifold Approximation and Projection (UMAP) algorithm with the RunUMAP function in Seurat. The FindAllMarkers function (test.use=bimod) in Seurat was used to identify the marker genes of each cluster. Once FindAllMarkers identified positive markers, they were manually annotated with reference to Gao et al. (2022) study and CellMarker 2.0 (https://ngdc.cncb.ac.cn/databasecommons/database). To trace the general development of related clusters, CytoTRACE (version 0.3.3) was applied, and monocle package (version 2.22.0) was used for in-depth analysis of development. The UMAP algorithm was continuously applied for a dimension reduction of subclusters. The R packages of GO.db (version 3.14.0), msigdbr (version 7.5.1), and GSVA (version 1.42.0) were included in the process of functional analysis. CellChat (version 1.6.1) and its dependencies were mainly used in cell interaction analysis. R version 4.1.2 was mainly used in our study, and final visualization and color optimization were adjusted by ggplot2 (version 3.4.4), RColorBrewer (1.1-3), and ggsci (3.0.0).

### 2.6 Hematoxylin-eosin (HE) staining

Mice liver specimens were fixed with 4% paraformaldehyde (PFA) and embedded in paraffin. Briefly,

liver sections were stained with hematoxylin solution for 5 min after deparaffinization and rehydration. Then, the liver sections were dipped in 1% acid ethanol for several times, and eosin solution was used to stain the sections for 3 min. Finally, the sections were dehydrated and mounted for photography.

**2.7 Primary cell flow cytometry (FCM)**

Mice were executed by bloodletting from the eyeball 12 h after the intraperitoneal injection of LPS. The livers and lower limb bones were extracted after saline infusion and placed in RIPM 1640 (Gibco, Waltham, MA, USA) supplemented with 10% fetal bovine serum (FBS, Gibco). Whole liver was pounded and digested with 0.05% collagenase IV (Worthington Biochemical, Lakewood, Colorado, USA) for 45 min at 37℃. Mononuclear cells in the liver were purified by Percoll (Cytiva, Uppsala, Sweden) after filtration, centrifugation and erythrocyte lysis. Mononuclear cells located in the middle layer were transferred to RIPM 1640 with 10% FBS. After centrifugation and resuspension with phosphate buffered saline (PBS; Servibio, Wuhan, China), the cells were prepared well for detection. Regarding the extraction of bone marrow (BM) cells, the bones were stripped and cleaned with PBS. Both ends of the bones were cut off, and the BM cells were flushed out by PBS perfusion. The long epiphyseal ends were ground and filtered before transferring to perfusate. The cells were counted and prepared for detection after erythrocyte lysis. Four FCM antibodies were used to label the target cells, including FITC-Cd45 (S18009F; Biolenged, San Diego, CA, USA), PE-Cd11b (M1/70; Biolenged), APC-Ly6g (1A8; Biolenged), and PC7-F4/80 (BM8; Biolenged). Antibodies were added to each sample tube according to the instructions. Black tube, single dye tube, and fluorescence minus one (FMO) tubes were set for precision analysis. The specimens were filtrated and detected on a flow cytometer (Beckman CytoFLEX; Beckman Coulter, Pasadena, CA, USA) after incubation at 4 for 30 min in the dark.

**2.8 Quantitative real time-PCR (qPCR)**

Total RNA was extracted from livers of different ages using TRIzol (Invitrogen, Waltham, MA, USA). RNA (1 mg at most) was reverse transcribed into cDNA using an RT Reagent Kit and genomic DNA (gDNA) Eraser (Takara, Osaka, Japan) according to the manufacturer's instructions. qPCR was conducted using TB Green Premix Ex Taq (TaKaRa) on a QuantStudio 7 Flex system (Life Technologies, USA). All samples were run in triplicate. Data were normalized to the expression level of glyceraldehyde-3-phosphate dehydrogenase (*Gapdh*) to quantify the relative expression of mRNA. The primers used are listed in Table S1.

**2.9 Western blotting**

Tissues and cells were collected and lysed using lysis buffer (Beyotime, Shanghai, China) with protease inhibitor (Yeasen, Shanghai, China). The concentrations of protein were detected by Pierce™ BCA Protein Assay Kits (Thermo Fisher, Waltham, MA, USA). A total of 20 μg protein per sample was separated via sodium dodecyl sulfate-polyacrylamide gel electrophoresis (SDS-PAGE) (EpiZyme, Shanghai, China) and blotted onto a 0.45 μm polyvinylidene difluoride (PVDF) membrane (Merck Millipore, Burlington, MA, USA). The membrane was blocked with 5% milk for 1 h at room temperature. Then, the membrane was incubated with primary antibody (interleukin-1β, IL-1β, A22257, ABclonal, Wuhan, China, 1:1000; tumor necrosis factor-α, TNF-α, A24214, ABclonal, 1:1000, glyceraldehyde-3-phosphate dehydrogenase, GAPDH, A19056, ABclonal, 1:5000; inducible nitric oxide synthase, iNOS, CY5993, Abways, 1:1000) at 4℃ overnight. The membrane was incubated with a horseradish peroxidase (HRP)-conjugated secondary antibody (anti-rabbit and anti-mouse, Cell Signaling Technology, Danvers, MA, 1:2000) for 1 h at room temperature after washing three times with Tris-buffered saline containing Tween 20 (TBST). The bands were visualized by a chemiluminescence system and was quantified by ImageJ software.

**2.10 Statistical analysis**

All calculations were performed with GraphPad Prism software (GraphPad, La Jolla, CA, USA). Original data were presented as means±standard deviation (SD), while standardized data were presented by

means±standard error of mean (SEM). Statistical analysis was performed using the unpaired two-tailed Student's *t* test for two-group comparisons. One-sample two-tailed t test was performed to examine the efficacy of control groups. The significance levels are presented as follows: $^{*}$ $P$<0.05, $^{**}$ $P$<0.01, and $^{***}$ $P$<0.001; ns indicates no statistical significance.

## 3 Results

### 3.1 Intrauterine hyperglycemia disrupts cell components and fetal liver development

After the maternal blood glucose achieved the target levels, fetal liver was collected at E18.5 as described in the methods for scRNA-seq (Fig. 1a). After quality control, a total of 6782 cells in Ctrl-F1 and 7380 cells in IHG-F1 male offspring were finally enrolled. Qualified cells were grouped into 16 clusters using the UMAP at a resolution of 0.5 (Figs. S1a and S1b). The detailed features of each cluster were presented in Figs. S1c-S1f. In UMAP clustering, the cell composition of the two groups was different. Myeloid polarization was shown in IHG-F1, manifesting as an increase in proportion of granulocyte-monocyte progenitor (GMP), monocyte_progenitor, neutrophil_1 (defined by *Ltf*, *Ngp*, *Lcn2*, *Anxa1*, and *Wfdc21*), neutrophil_2 (defined by *Mmp8* and *Thbs1*), and neutrophil_3 (defined by *Chil3* and *Pglyrp1*; Figs. 1b, 1c, and S1c). In contrast, the number and proportion of B cell and erythroid cell lineages in IHG-F1 was decreased. Moreover, we observed a group of Macro+ resident macrophages as early as E18.5 in the fetal liver, and its augment in IHG-F1 was quite distinct (Fig. 1b).

Given that the fetal liver has a certain hematopoietic function, we were curious about whether the myeloid polarization in IHG-F1 was related to hematopoietic anomaly caused by IHG exposure. Using the Cyto TRACE, we analyzed the general development of 16 clusters in merged samples (Fig. 1d). Three major groups were mainly sorted out according to their developmental lineage: the sequence of the myeloid lineage group (GMP, monocyte_progenitor, neutrophil_3, neutrophil_1, neutrophil_2), the B cell lineage group (B_cell_4, B_cell_3, B_cell_2, B_cell_1), and the erythroid cell lineage group (Erythroid_cell_4, Erythroid_cell_2, Erythroid_cell_3, Erythroid_cell_1). The B cell and erythroid cell lineages in IHG-F1 presented a trend of retarded development (Figs. 1e and f). These results indicate that IHG may affect fetal hepatic cell component, mainly manifested as myeloid polarization. Moreover, many immune cells in the fetal liver showed the hypo-development when exposed to IHG.

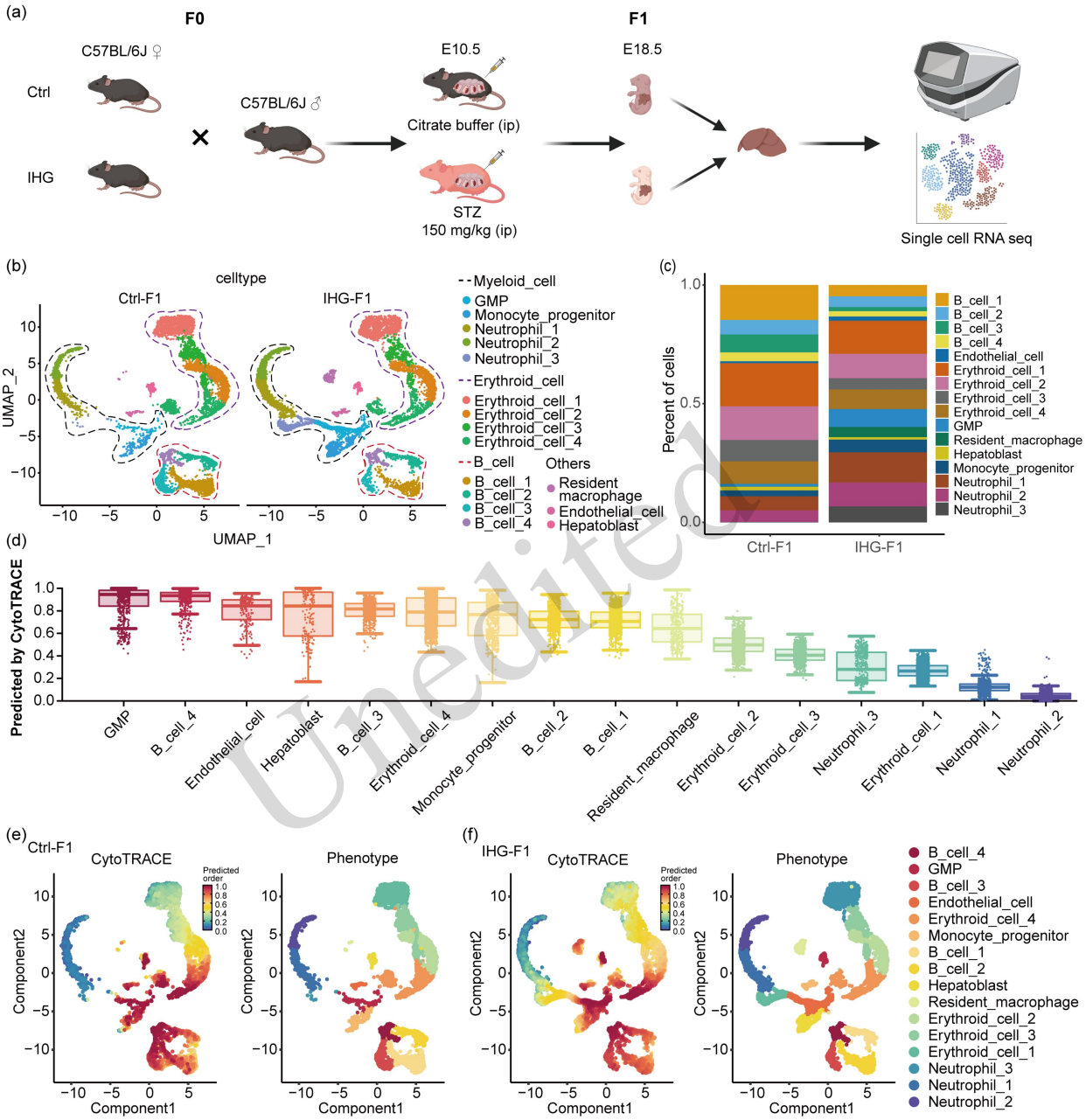




**Fig. 1** Intrauterine hyperglycemia disrupts cell components and the development of fetal liver. **(a)** Procedure of IHG model building and fetal liver scRNA-seq. **(b)** Cell components of UMAP analysis in Ctrl-F1 and IHG-F1 groups. **(c)** Percentage of cell clusters in Ctrl-F1 and IHG-F1 groups. **(d)** The Cyto TRACE predicts the development of 16 clusters in merged samples. **(e, f)** The Cyto TRACE of Ctrl-F1 and IHG-F1. IHG: intrauterine hyperglycemia; scRNA-seq: single-cell RNA sequencing; UMAP: Uniform Manifold Approximation and Projection; STZ: streptozotocin; GMP: granulocyte-monocyte progenitor.

### 3.2 Intrauterine hyperglycemia induces the development retardation of multiple cell lineages in fetal liver

To explore the precise changes in these immune-related components, pseudotime analysis was performed. Firstly, myeloid clusters, including GMP, monocyte_progenitor, neutrophil_3, neutrophil_1, and neutrophil_2, were enrolled for analysis except for resident macrophages. GMP differentiated into two terminals: one was the mononuclear phagocyte system (MPS), and the other was granulocytes (Fig. 2a and 2b). We found that the development of granulocytes was relatively mature in the E18.5 fetal liver, while the MPS still remained in the

progenitor stage. We extracted several key genes to describe the development process of myeloid lineage in the fetal liver according to the study of Xie et al. (2020). Then, four stages of myeloid granulocyte development were proposed: GMP period-*Prtn3* and *Elane*; neutrophil_3 period-*Chil3*; neutrophil_1 period-*Ltf* and *Ngp*; neutrophil_2 period-*Retnlg*, *Mmp8*, and *S100a9* (Figs. 2c and 2d). The expression level of myeloid precursor genes (*Prtn3* and *Elane*) was continuously downregulated during the pseudotime process (Fig. 2c), while the expression of terminal stage genes, such as *Retnlg*, *Mmp8*, and *S100a9*, continued to rise (Fig. 2d).

As shown in Fig. 2e, after sample splitting, there were more GMP and neutrophil_3 (early stage) but less mature neutrophil_1 and neutrophil_2 cells in the IHG-F1 myeloid lineage. Figs. 2f and 2g show the expression levels of these key genes in individual cells of different samples. It can be seen that the main population of Ctrl-F1 is located in the end period of development, while the main population of IHG-F1 is in the middle stage of development, which indicates the myeloid lineage developmental retardation of IHG-F1 at the gene level. Fig. S2 was referred to the study of Lee et al. (2021), which generally depicts the pre-BCR-dependent proliferation to V(D)J rearrangement stage of our samples. The pseudotime analysis shows the developmental sequence of the four clusters of B cell lineage (Figs. S2a and S2b). Although the diminution of B cell lineage in IHG-F1 may affect the identification of its developmental state (Figs. 1b and 1c), we could still recognize that the terminal population was dominated by Ctrl-F1 with the cue of key genes (Figs. S2c-S2e). Similarly, Fig. S3 suggests a potential erythroid cell lineage retardation in IHG-F1 (Table S2). Above all, IHG exposure induced multiple lineages of fetal liver development retardation, of which the myeloid lineage was the most prominent.

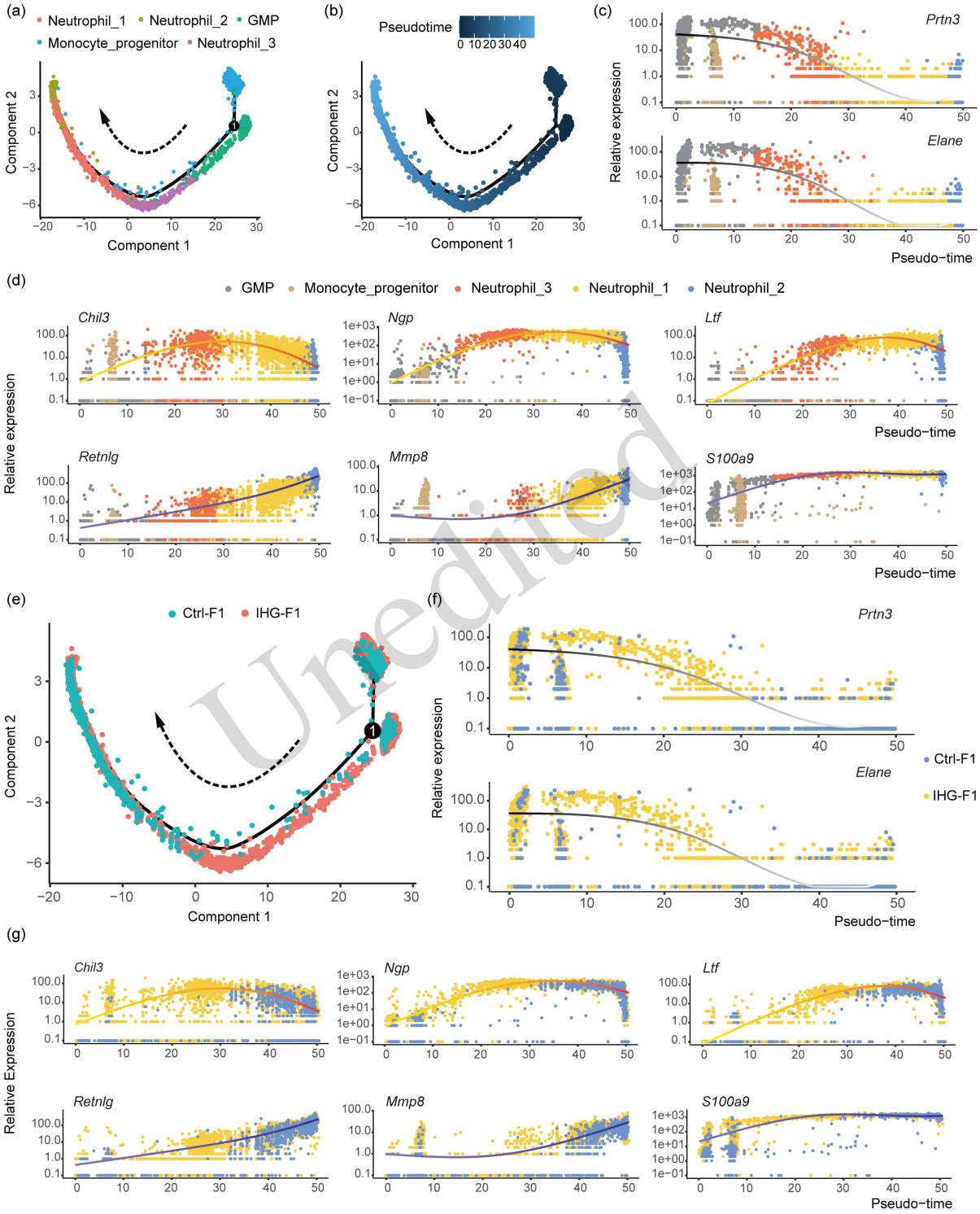


**Fig. 2** Intrauterine hyperglycemia induces myeloid lineage development retardation in the fetal liver. Pseudotime analysis by cell type **(a)** and pseudotime **(b)**. **(c)** Kinetic plots of myeloid precursor genes. **(d)** Kinetic plots of neutrophil markers according to the development trajectories. **(e)** Pseudotime analysis by groups. **(f)** Kinetic plots of myeloid precursor genes by groups. **(g)** Kinetic plots of neutrophil markers by groups. IHG: intrauterine hyperglycemia; GMP: granulocyte-monocyte progenitor; *Prtn3*: proteinase 3; *Elane*: elastase, neutrophil expressed; *Chil3*: chitinase-like 3; *Ngp*: neutrophil granular protein; *Ltf*: lactotransferrin; *Retnlg*: resistin-like molecule gamma; *Mmp8*: matrix metalloproteinase 8; *S100a9*: S100 calcium binding protein A9.

### 3.3 Intrauterine hyperglycemia affects the components and functions of myeloid lineage during adulthood

After the identification of the above effects of IHG on the fetal liver, we explored whether these effects persist into adulthood. When the offspring grew up to 8 weeks, three male mice were randomly sacrificed and pooled from each group for liver single cell sequence (denoted as Ctrl-F1 and IHG-F1) (Fig. 3a). Figs. S4a and S4b show the clusters after UMAP dimension reduction (merged samples), in which the main cell populations were B cells, natural killer (NK) cells, and monocytes. Among them, NK cells were not clustered in E18.5 fetal livers. Fig. S4c shows the key markers involved in cluster annotation. After sample splitting, the B cell population was relatively increased in IHG-F1, while the proportion of neutrophils and hepatocytes decreased (Figs. 3b and 3c). These results suggested that myeloid polarization in fetal offspring livers with IHG was restored to some extent during adulthood, though the cellular composition was apparently different from fetal livers.

Although the myeloid polarization was restored in adult offspring, we sought to further explore the effects of IHG exposure on myeloid components and functions. The monocyte cluster was divided into three subsets (0, 1, and 2) at a resolution of 0.1 (Fig. S4d). The distribution of monocyte subsets in two groups is shown in Fig. 3d. Fig. 3e illustrates key markers in two groups, and Fig. 3f represents the proportion of these three subsets in different groups. Cluster 0 accounted for a dominant proportion in Ctrl-F1, while cluster 1 ranked highest ratio in IHG-F1. Subsequent functional analysis demonstrated that cluster 0 monocytes displayed stronger antigen presenting ability, while cluster 1 monocytes showed relatively higher inflammatory cell chemotaxis function (Fig. 3g). Then, the differential expression genes (DEGs) of monocyte subcluster derived from two groups was analyzed. Although a few number of DEGs was identified, monocytes in the IHG-F1 group displayed a more typical macrophage phenotype with high expression of *F13a1*, *Hmox1* and *Lyz2* (Fig. S4e). To trace the potential origin of "hematopoietic memory", we intersected the upregulated DEGs of GMP and monocyte_progenitor in IHG-F1, and found that most upregulated genes in IHG-F1 were included (Fig. S4f).

Subsequently, the neutrophil cluster was analyzed, however, subsets were not recommended at a reasonable resolution, probably due to their small number (Figs. S5a and 5e). Interestingly, the number of neutrophils in IHG-F1 accounted for approximately 50% of that in the Ctrl-F1 group (Fig. S5b), but the markers representing neutrophils in IHG-F1 were obviously higher than those in Ctrl-F1 (Fig. S5c). In terms of function, neutrophils in IHG-F1 presented higher NETosis and chemotactic potential compared with Ctrl-F1 (Fig. S5d). DEGs analysis for neutrophils demonstrated that proinflammatory cytokine *Il-1β* was found to be highly expressed in IHG-F1, suggesting that inflammatory pre-stimulation may persists in IHG adult offspring (Fig. S5f). The enrichment analysis for neutrophils in different groups was shown in Fig. S5g. In this part, we identified that IHG can still impact the components and functions of myeloid lineage in the liver during adulthood.

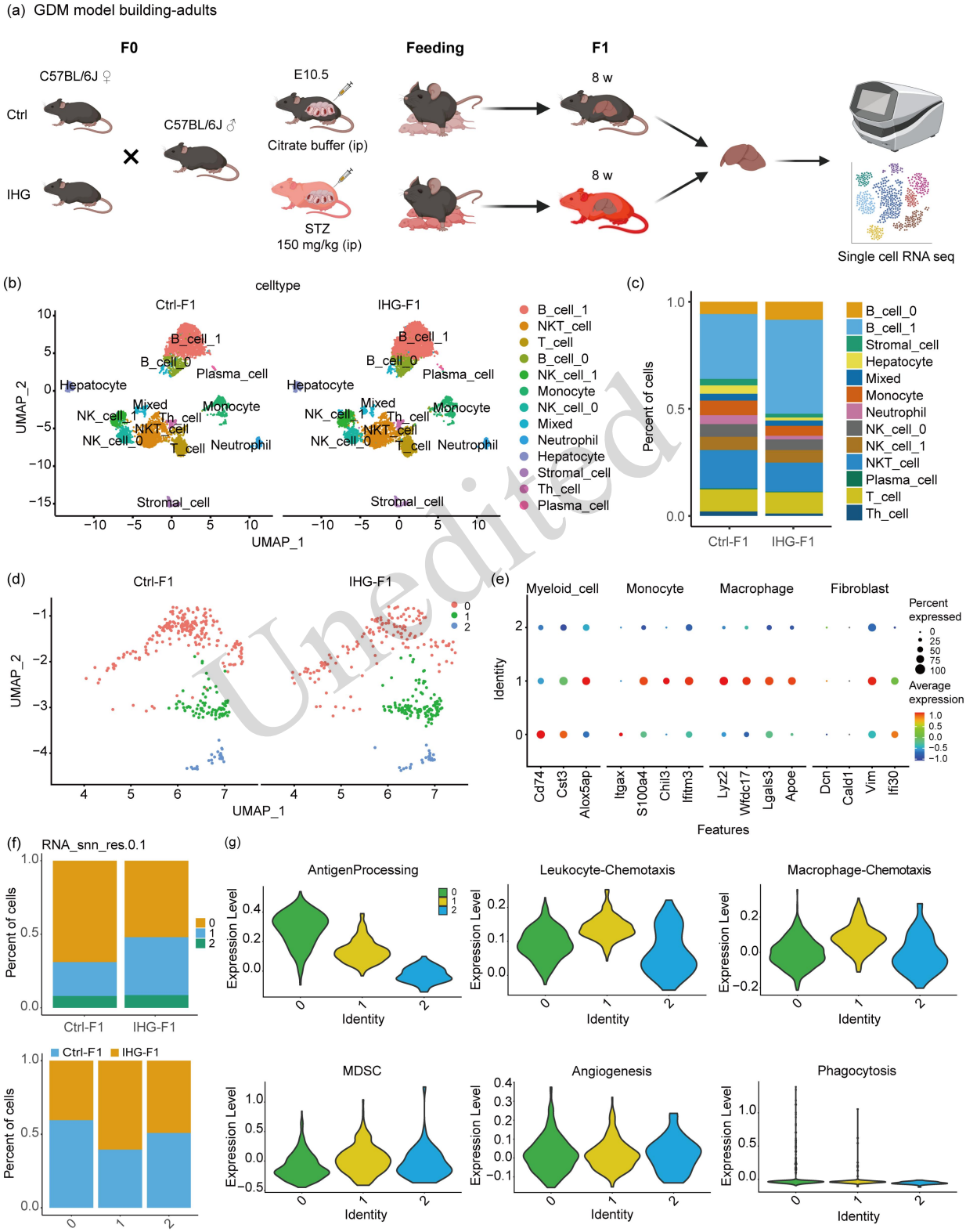


**Fig. 3** Intrauterine hyperglycemia affects the components and functions of myeloid lineage during adulthood. **(a)** Generation of adult male offspring and liver scRNA-seq. **(b)** Cell components of UMAP analysis in Ctrl-F1 and IHG-F1 groups. **(c)** Percentage of cell clusters in Ctrl-F1 and IHG-F1 groups. **(d)** Subclusters of monocytes in the Ctrl-F1 and IHG-F1 groups. **(e)** Key markers for

identification of monocyte subclusters. **(f)** Percentage of monocyte subclusters in IHG-F1 and Ctrl-F1 groups. **(g)** Monocyte function scoring in different clusters. IHG: intrauterine hyperglycemia; STZ: streptozotocin; scRNA-seq: single-cell RNA sequencing; UMAP: Uniform Manifold Approximation and Projection; NK cell: natural killer cell; Th cell: help T cell; MDSC: myeloid-derived suppressor cell.

### 3.4 Intrauterine hyperglycemia alters myeloid cell interactions in offspring liver in adulthood

We further explored the effects of IHG exposure on the interaction of liver cells in adult offspring by CellChat analysis. The global cell-cell interaction was enhanced in the IHG-F1 group (Figs. 4a, 4b, and Table S3). Furthermore, an increased number and intensity of interactions between monocytes and multiple clusters (especially the hepatic stromal cells) was observed in IHG-F1. The heatmap of cellular communication showed that the hepatic stromal cells, as the signal sender, significantly enhanced interactions with monocytes, hepatocytes, and neutrophils in IHG-F1 (Fig. 4c). Then, we performed a ligand-receptor pair analysis based on these differences in cellular interactions. As shown in Fig. 4d, the ligand-receptor pairs, such as vascular endothelial growth factor (VEGF), transforming growth factor β (TGF-β), thrombospondin (THBS), and bone morphogenetic protein (BMP) families, were increased in Ctrl-F1, while noncanonical WNT (ncWNT), vitronectin (VTN), TENASCIN, and fibronectin-1 (FN1) series pairs were elevated in IHG-F1, suggesting that matrix crosslinking-related functions were enhanced in IHG-F1.

Furthermore, the outgoing and incoming signaling of these ligand-receptor pairs was analyzed. It was found that COLLAGEN, FN1 and LAMININ signaling were obviously enhanced in the interaction between monocyte and hepatic stromal cell in the IHG group. In contrast, the THBS signaling interacting in neutrophil and hepatic stromal cells was strengthened in Ctrl-F1 (Fig. 4e). Specifically, Figs. S6a-S6d demonstrated the interaction differences of COLLAGEN, FN1, LAMININ, and THBS signaling between the two groups, and Figs. S6e-S6h present the differences in the expression of ligand-receptor pairs for the four signaling families between Ctrl-F1 and IHG-F1 groups. These findings based on CellChat suggest that IHG alters myeloid cell interactions in the liver of adulthood offspring.

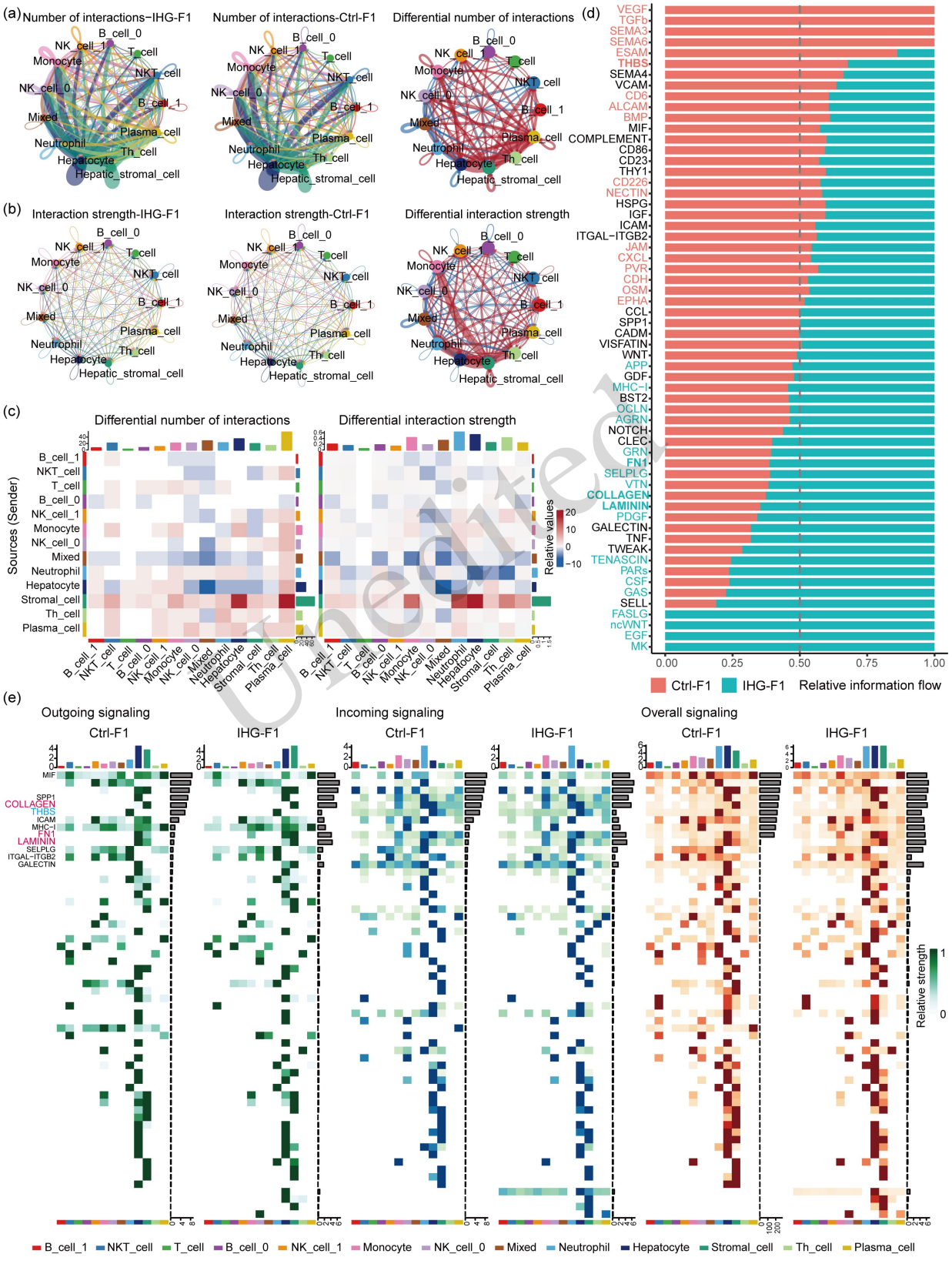


**Fig. 4** Intrauterine hyperglycemia alters myeloid cell interactions in the adult offspring liver. **(a)** Number of interactions and differences between the Ctrl-F1 and IHG-F1 groups. **(b)** Strength of interactions and differences between Ctrl-F1 and IHG-F1

groups. **(c)** Different interactions annotated by senders. **(d)** Enrichment analysis of interaction pairs. **(e)** Outgoing, incoming, and overall interaction signaling analysis. IHG: intrauterine hyperglycemia; NK cell: natural killer cell; Th cell: help T cell.

### 3.5 Intrauterine hyperglycemia disrupts the response of hepatic myeloid cells to LPS-induced sepsis in adult offspring

According to previous findings, we hypothesized that offspring exposed to IHG may be more susceptible to deficiencies in defense against acute infections. Thus, adult offspring were arranged for sepsis model construction (Fig. 5a). Mice were sacrificed 12 h after LPS intraperitoneal injection. Firstly, we found that the infiltration of inflammatory cells in the liver was significantly increased in the IHG-F1 group (Fig. 5b). Furthermore, we extracted BM and hepatic primary cells from LPS-induced sepsis offspring for flow cytometry. Here, Cd11b was used to label myeloid mononuclear cells, Cd11b+F4/80 to label macrophages, and Ly6g to label neutrophils. The proportion of $Cd11b^{+}$ myeloid mononuclear cells in the BM of IHG-F1 group was significantly increased (Figs. 5c and 5d), along with its mean fluorescence intensity (MFI) (Fig. 5e). The proportion of $Cd11^{+}$ $F4/80^{+}$ macrophages in IHG-F1 BM decreased (Figs. 5f and 5g), but this was accompanied by an increase in $Ly6g^{+}$ neutrophils (Figs. 5h and 5j).

Next, we explored how these cell populations reacted in the liver. After LPS injection, the ratio of neutrophils tended to increase in the IHG-F1 group, although the increase was not statistically significant (Figs. 5j and 5k). In contrast, the MFI of Ly6g in IHG-F1 offspring significantly decreased (Fig. 5l). The alterations of macrophages and myeloid mononuclear cells were also observed in the BM of Ctrl-F1 and IHG-F1 (Figs. 5m-5p). In this part, we demonstrated that IHG exposure may affect the response of myeloid cells to LPS-induced sepsis.

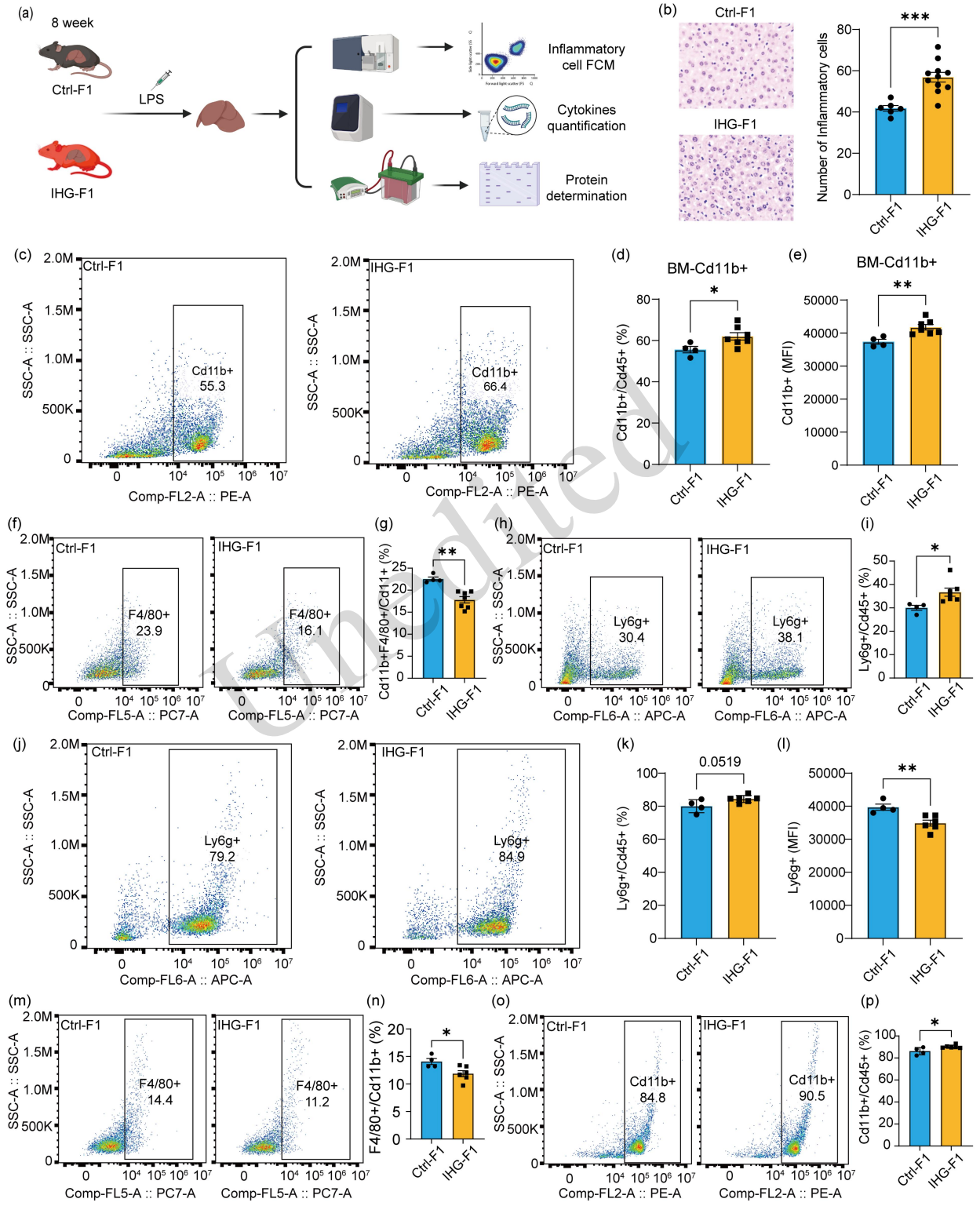


**Fig. 5** Intrauterine hyperglycemia disrupts the response of offspring liver myeloid cells to LPS-induced sepsis. **(a)** Procedure of LPS-induced sepsis model building. **(b)** Inflammatory cell infiltration in the Ctrl-F1 and IHG-F1 groups. **(c)** Pseudo-color plot of Cd11b+ monocytes in the BM of Ctrl-F1 and IHG-F1 groups. Proportions of Cd11b+/Cd45+ **(d)** and MFI of Cd11b+ (**e**) in the BM of Ctrl-F1 and IHG-F1 groups. **(f)** Pseudo-color plot of Cd11b+F4/80+ macrophages in the BM of Ctrl-F1 and IHG-F1 groups. **(g)**

Proportions of Cd11b+F4/80+/Cd11b+ in the BM of Ctrl-F1 and IHG-F1 groups. **(h)** Pseudo-color plot of Ly6g+ neutrophils in the BM of Ctrl-F1 and IHG-F1 groups. **(i)** Proportions of Ly6g+/Cd45+ in the BM of Ctrl-F1 and IHG-F1 groups. **(j)** Pseudo-color plot of Ly6g+ neutrophils in the livers of Ctrl-F1 and IHG-F1 groups. Proportions of Ly6g+/Cd45+ (**k**) and MFI of Ly6g+ (**l**) in the livers of Ctrl-F1 and IHG-F1 groups. **(m)** Pseudo-color plot of Cd11b+F4/80 macrophages in the livers of Ctrl-F1 and IHG-F1 groups. **(n)** Proportions of Cd11b+F4/80/Cd11b+ in the livers of Ctrl-F1 and IHG-F1 groups. **(o)** Pseudo-color plot of Cd11b+ monocytes in the livers of Ctrl-F1 and IHG-F1 groups. **(p)** Proportions of Cd11b+/Cd45+ in the livers of Ctrl-F1 and IHG-F1 groups. LPS: lipopolysaccharide; IHG: intrauterine hyperglycemia; Cd: cluster of differentiation; MFI: mean fluorescence intensity; BM: bone marrow; FCM: flow cytometry. $^{*}$ $P$<0.05, $^{**}$ $P$<0.01, and $^{***}$ $P$<0.001. The values are expressed as mean± standard error of the mean (SEM), n≥3.

### 3.6 Intrauterine hyperglycemia induces deficient acute-phase response to LPS in offspring

Finally, we investigated whether this disordered response to LPS-induced sepsis in IHG-F1 was associated with cytokines in the liver. Interleukin-6 (*IL-6*), monocyte chemoattractant protein-1 (*Mcp-1*), and C-X-C chemokine receptor type 2/4 (*Cxcr2/4*) were found to be transcriptionally elevated in the livers of the IHG group without LPS, suggesting an underlying increase in the inflammatory levels in IHG offspring (Fig. S7a). However, there were no significant differences in the transcription and translation levels of IL-1β, TNF-α and iNOS (Fig. S7b-S7d). To our surprise, when LPS was used to form the sepsis model, a large number of inflammatory factors (*TNF-α*, *IL-1β*, *iNOS*, *Mcp-1*, and *Cxcr2/4*) showed transcriptional decline in the liver tissue of offspring with IHG exposure (Fig. 6a). Meanwhile, in the IHG-F1 group, acute-phase response cytokines TNF-α, IL-1β, and iNOS were significantly reduced at the protein level (Figs. 6b-6d). These results indicate that IHG exposure may cause deficiency of hepatic acute-phase response to infection in adult offspring.

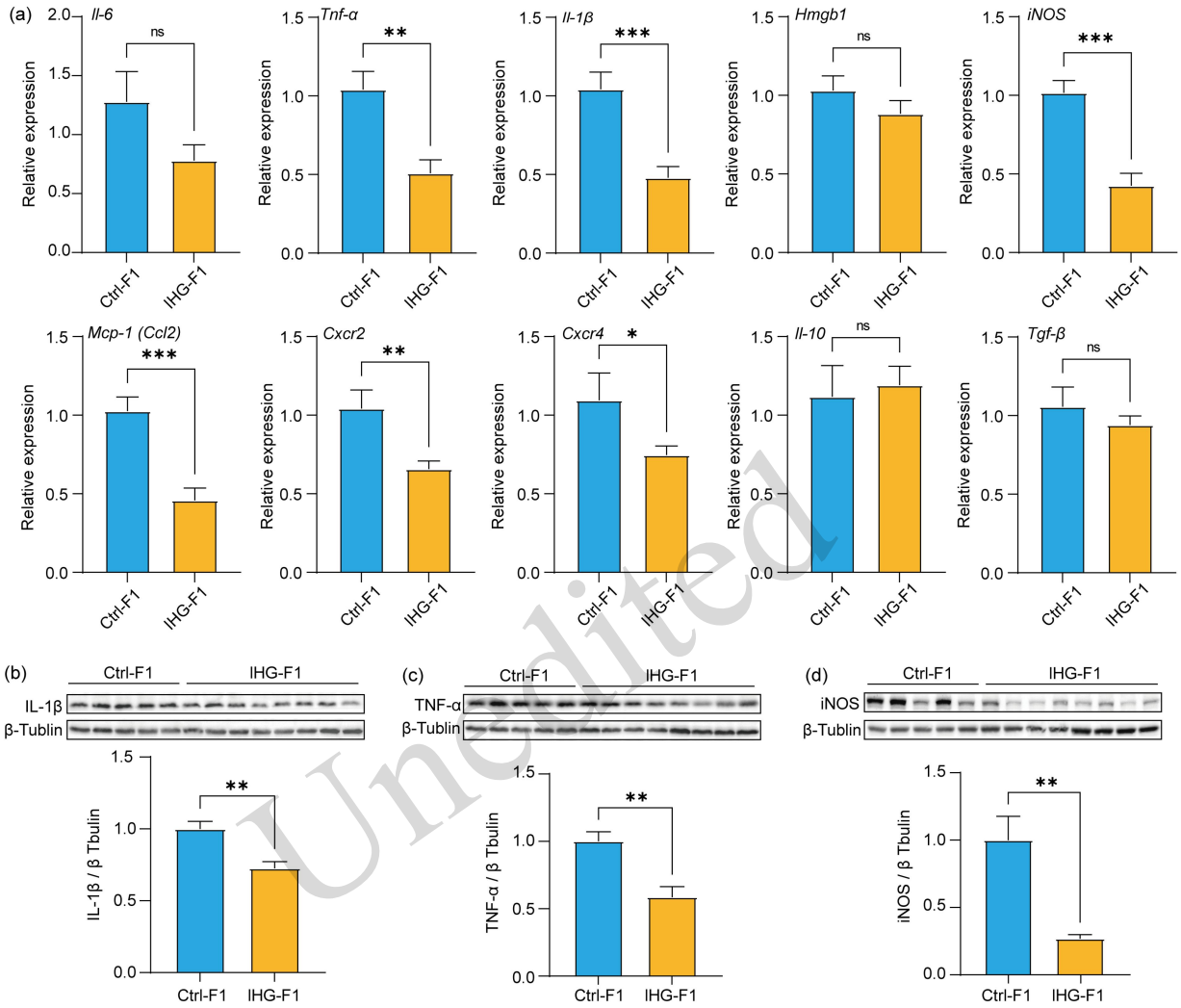


**Fig. 6** Intrauterine hyperglycemia leads to acute-phase response deficiency in LPS-induced sepsis. **(a)** Relative mRNA expression level of acute-phase response cytokines in the livers of Ctrl-F1 and IHG-F1 groups. Western blotting analysis of IL-1β **(b)**, TNF-α **(c)**, and iNOS **(d)** in the liver tissue of Ctrl-F1 and IHG-F1 groups. LPS: lipopolysaccharide; mRNA: message RNA; IHG: intrauterine hyperglycemia; IL-1β: interleukin-1β; TNF-α: tumor necrosis factor-α; iNOS: inducible nitric oxide synthase; *Il-6*: interleukin-6; *Hmgb1*: high mobility group box-1 protein; *Mcp-1*: monocyte chemoattractant protein-1; *Cxcr2*: C-X-C motif chemokine receptor 2; *Cxcr4*: C-X-C motif chemokine receptor 4; *Il-10*: interleukin-10; *TGF-β*: transforming growth factor β; * $P$<0.05, ** $P$<0.01, and *** $P$<0.001; ns: not significant. The values are expressed as mean±standard error of the mean (SEM), n≥3.

## 4 Discussion

To our knowledge, this study is the first to portray a liver single-cell atlas for offspring with IHG. Interestingly, we found that this adverse intrauterine exposure impacts the composition, development, and function of myeloid lineage in the liver, which may lead to deficient response to acute infections. As a temporary hematopoietic organ, the liver undertakes the transition of hematopoietic function to BM at the fetal period.[22] In our study, myeloid polarization was found in the fetal livers (E18.5) of offspring with IHG exposure. Myeloid polarization has been widely reported in the realm of diabetes mellitus research at the single-cell level (Zakharov et al., 2020; Zhong et al., 2022). In a STZ-induced type 1 diabetes (T1D) mouse model, dysregulation of the neutrophil/B cell ratio in BM could lead to susceptibility to osteopenia (Zhong, et al., 2022). Recently, sc-RNA sequencing focusing on the characteristics of placental and umbilical cord blood in human

GDM has emerged (Yang, et al., 2021; Yin, et al., 2024). Yin, et al. (2024) analyzed the single-cell transcriptional data of cord blood mononuclear cells from the fetuses of healthy and GDM mothers, and found that monocytes in the cord blood of GDM mothers featured expanded CXCL8+IL1β+ subclusters, which share a similar phenotype with atherosclerosis. By coincidence, another study has confirmed that "hematopoietic memory" derived from IHG can affect the long-term health of offspring (Govindarajah, et al., 2024). The expansion of myeloid hematopoietic precursors conferred a predisposition to atherosclerosis in *Apoe*$^{-/-}$ offspring mice with GDM mothers (Govindarajah, et al., 2024). Based on these findings, we supposed that IHG dose aggravates the myeloid expansion of hematopoietic cells. However, certain questions are posed here. Firstly, we are concerned about the durability and befitting functions of polarization or expansion. Whether this premature overload of myeloid progenitors depletes their longevity and reactive expansion is still unknown; nonetheless, myeloid related deficiency was observed both in our study and Govindarajah, et al. (2024), when it comes to the LPS-induced sepsis. Furthermore, accompanied by the reduction or insufficiency of other lineages (erythroid and B cells), this abnormal expansion disrupts the developmental balance of hematopoietic cells in the fetal liver. Nevertheless, the long-term effects of these reduced or underdeveloped progenitors on the offspring with IHG exposure remain unclear.

In relation to the issue of hematopoietic development, we observed that various cell populations within the livers of fetuses affected by IHG exhibited developmental delays. In the context of the STZ model, the primary consideration is the overarching developmental delay. According to our team's prior experience, neonatal mice born following STZ-induced modeling frequently present as small for gestational age (SGA), which may be attributable to the nutritional restrictions associated with the maternal disease state. Similarly, STZ-induced maternal hyperglycemia leads to reduced blood glucose levels in neonatal offspring, resulting in growth restriction (Gong et al., 2024). However, it is well recognized that in clinical cases of GDM, there is an increased prevalence of large for gestational age (LGA) infants in this population. This phenomenon may be attributed to the inherent limitations of the STZ model, which fails to accurately replicate the blood glucose levels typically observed in gestational diabetes. Besides, the specific hematopoietic status of these infants remains unclear. It is important to acknowledge the inherent limitations in studying hematopoietic development at the specific gestational age of E18.5. Studies have indicated that the proportion of hematopoietic stem cells (HSCs) in the cord blood of neonates born to mothers with GDM is elevated (Hadarits et al., 2016; Zhang et al., 2024), implying that their differentiation and proliferation may be subject to inhibition. Given that glucose metabolism regulates the initiation and magnitude of HSCs induction *in vivo* (Harris et al., 2013), elucidating the metabolic pathways involved in cell proliferation and differentiation is crucial for optimizing culture conditions for HSCs. Regrettably, the impact of high glucose on myeloid hematopoietic function remains to be explored, necessitating further *in vivo* and *in vitro* investigations to explore this phenomenon. More importantly, to accurately elucidate the nuances of hematopoietic development in the context of GDM, investigations across multiple time points and various hematopoietic organs during embryonic development are imperative. Nonetheless, our findings reveal that multiple lineages of hematopoietic cells exhibit developmental delays in IHG, underscoring the significance of this research.

In our study, myeloid polarization was restored in the adult offspring livers with IHG; the proportion of monocytes and neutrophils were not elevated as they were in the fetal liver. However, during the subset analysis, differences in myeloid cells were found between the two groups, with cluster 1 dominating in IHG and cluster 0 in the Ctrl group. Subsequent functional analysis also suggested the discrepancy between them. In fact, cluster 1 subset possessed obvious macrophage phenotypes (both in markers and functions) with activated inflammatory chemotaxis and matrix interaction features. Moreover, CellChat demonstrated that the interactions between monocytes and hepatic stromal cells was enhanced in adult offspring with IHG. The signaling pathways related to extracellular matrix formation (COLLAGEN, FN1, and LAMININ) were significantly upregulated. Therefore, we speculated that the offspring of IHG may be susceptible to non-alcoholic liver disease and hepatic fibrosis under this immune microenvironment, though further studies are needed to supplement this hypothesis. Since we defined a group of macrophages, namely hepatic resident macrophages during the fetal liver period, the origin of these monocytes in the liver of offspring with IHG mother was considered. These resident cells were significantly increased in the fetal liver of IHG offspring, but it is unclear whether cluster 1 dominating in adult offspring liver of IHG originated from these. Hepatic resident macrophages labeled Macro$^{+}$ were reported to protect against commensal-driven liver inflammation (Miyamoto et al., 2024). Therefore, it seems to be worthwhile to explore their characteristic once they are exposed to IHG during the developmental period. On

the other hand, neutrophil numbers were reduced in the adult offspring liver of IHG, compared with the Ctrl group. In contrast, the expression level of *Il-1β* was significantly increased in neutrophils of IHG offspring, suggesting an activated inflammatory state. Subsequent analysis of CellChat demonstrated that the THBS family-related ligand-receptor pairs were significantly downregulated in neutrophils of IHG offspring. Studies have confirmed that THBS-1 deficient (*Thbs1*$^{-/-}$) mice exhibited a hyperinflammatory response in multiple pulmonary infections (Zhao et al., 2015; Penaloza et al., 2021). In summary, though myeloid polarization was restored to some extent in the livers adult offspring with IHG, the proinflammatory potential of these myeloid cells seemed to be deeply imprinted with the so-called "hematopoietic memory." (Govindarajah, et al., 2024) However, our work tended to be rather descriptive and failed to track the development of the myeloid lineage dynamically in offspring with IHG. Thus, limitations in undertanding the relevant mechanism must be acknowledged.

The LPS-induced sepsis model was established to further evaluate the function of myeloid lineage in adult offspring with IHG. The proportions of myeloid cells and neutrophils were increased in IHG offspring after LPS induction, although this was accompanied by a reduction in macrophages. Increased infiltration of inflammatory cells in liver sections of IHG offspring was also observed. The qPCR and WB of liver tissue demonstrated that many inflammatory factors and acute-phase response cytokines were significantly reduced in the IHG group compared with the Ctrl group, indicating defects against acute infection. The study conducted by Govindarajah et al. also found that inflammatory cytokine concentration in the offspring serum of IHG was reduced after LPS treatment, consistent with our findings ((Govindarajah et al., 2024). The authors speculated that this reduction might be due to pyroptosis caused by hyperaction of inflammatory signaling after the LPS hit, but in fact, the reduction in macrophages was validated in our study. We attempted to explain this phenomenon as "macrophage phagocytosis of neutrophil extracellular traps (NETs) deficiency", whereas the marker of NETs, namely citrullinated histones, cannot been stained well (data not shown). We hypothesized that the real root of the defect was the abnormal expansion of myeloid progenitors. These progenitors exposed to hyperglycemia were activated early in utero. The "hematopoietic memory" might foster and persist even in adulthood, manifesting mild inflammatory state at baseline, though multiple mechanisms should be explored. As indicated in Fig. S7, the transcription level of inflammatory factors in the offspring liver of IHG was elevated without LPS stimulation. However, myeloid reprogramming triggered by western diet was reported to be enhanced during LPS treatment, which was opposite to the findings of IHG exposure (Christ et al., 2018). Thus, the mechanism of deficiency originating from the "hematopoietic memory" remains unclear. Inspired by the above perspectives, in future work, we will focus on the functional and differential orientation of these myeloid progenitors derived from offspring of IHG mother in the context of inflammatory diseases.

## 5 Conclusions

Our study has mapped the first single-cell profile of mouse liver with IHG. Here, myeloid polarization was identified in the fetal liver of IHG offspring, accompanied by the developmental retardation of multiple cell lineages. Sc-RNA analysis for adult offspring liver revealed different components and functions of myeloid cells between Ctrl and IHG groups. Lastly, the LPS-induced sepsis model validated the deficiency in acute-phase response when the adult offspring was once exposed to IHG (Fig. 7).

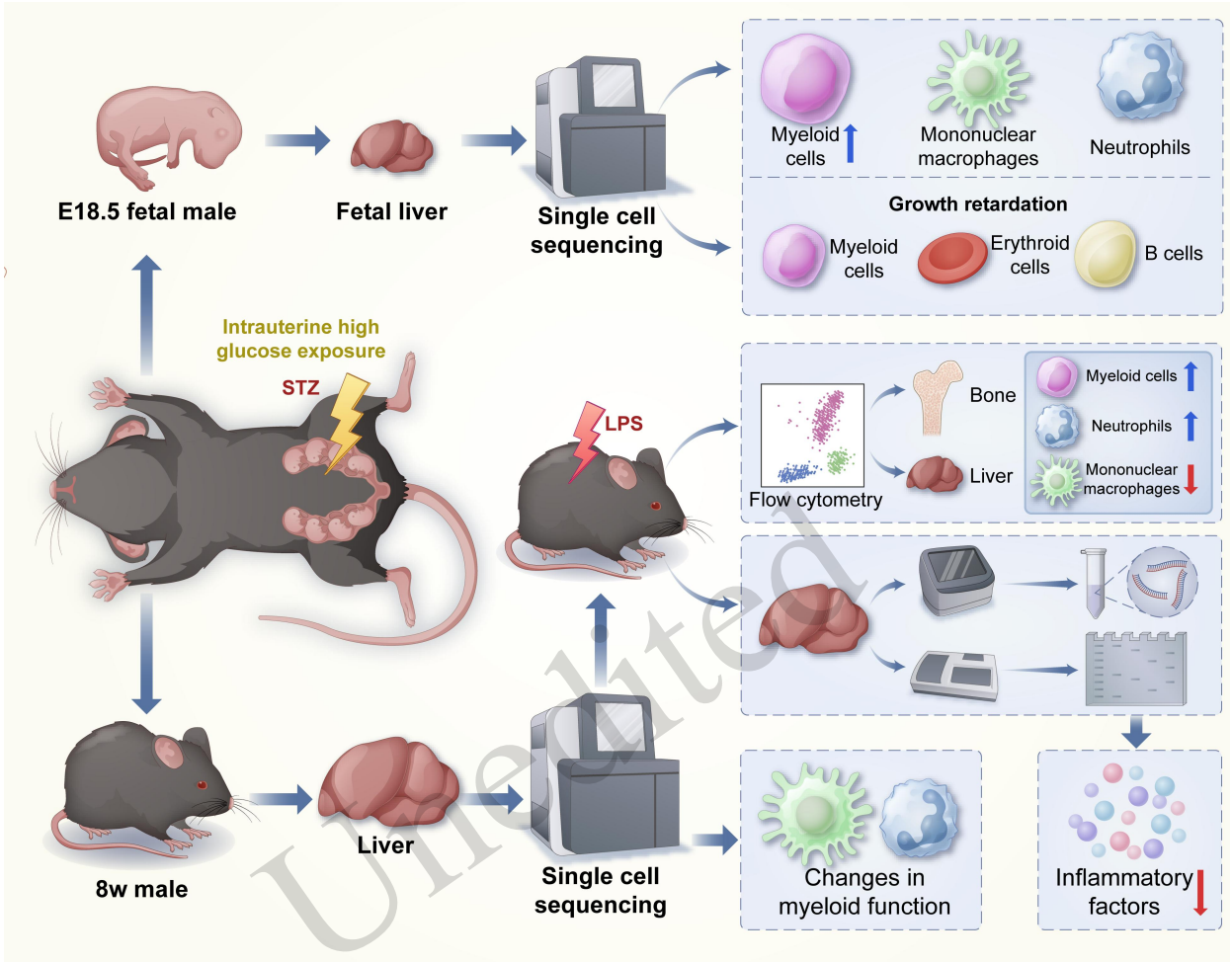


**Fig. 7** Graphical abstract of our research. STZ: Streptozotocin.

## Data availability statement

All datasets generated and analyzed during this study are included in this published article and its Supplementary information files. Sequence data that support the findings of this study have been deposited in the Gene Expression Omnibus (GEO) with the primary accession of GSE289783. The private access token for distribution to reviewers is **gfeziciunpaflkb**.

## Acknowledgments

This work is supported by the National Natural Science Foundation of China (No. 82088102), CAMS Innovation Fund for Medical Sciences (No. 2019-I2M-5-064), Collaborative Innovation Program of Shanghai Municipal Health Commission (No. 2020CXJQ01), Key Discipline Construction Project (2023-2025) of Three-Year Initiative Plan for Strengthening Public Health System Construction in Shanghai (No. GWVI-11.1-35), Shanghai Clinical Research Center for Gynecological Diseases (22MC1940200), Shanghai Urogenital System Diseases Research Center (No. 2022ZZ01012) and Shanghai Frontiers Science Research Center of Reproduction and Development. Key Laboratory of Reproductive Genetics, Ministry of Education, Zhejiang University, Hangzhou, Zhejiang Province, P.R. China (No. ZDFY2024-RG-1). This work was supported by the Medical Science Data Center of Fudan University. We also appreciated the animal experimental platform provided by Shanghai Model Organisms (Shanghai, China), the sc-RNA seq service supported by Oebiotech (Shanghai, China).

## Author contributions

Hefeng HUANG and Hong ZHU designed and conceptualized the whole work. Jiahang MO, Jing YAN, and Yi CHENG performed experiments performed experiments and wrote the manuscript. Kaixuan DONG, Jing YAN, and Jie LI helped conduct the experiments of mice model. Tianyou WANG and Jiahang MO participated in data analysis and figure preparation. Meijun

PAN and Guolian DING revised the manuscript. Hefeng HUANG and Hong ZHU supervision, project administration, and funding acquisition. All authors approved the final version of the manuscript for submission.

## Compliance with ethics guidelines

Jiahang MO, Jing YAN, Yi CHENG, Kaixuan DONG, Tianyou WANG, Jie LI, Meijun PAN, Guolian DING, Hong ZHU, Hefeng HUANG declare that they have no conflict of interest.

All procedures for animal experiments were conducted in accordance with the Guide for the Care and Use of Laboratory Animals at Shanghai Model Organisms (Shanghai, China) (approval ID for the animal IACUC protocol: 2019-0026).

## References

Bianco, M.E., Josefson, J.L., 2019. Hyperglycemia during pregnancy and long-term offspring outcomes. *Curr. Diab. Rep.*, **19**(12):143. https://dx.doi.org/10.1007/s11892-019-1267-6

Butler, A., Hoffman, P., Smibert, P.*, et al.*, 2018. Integrating single-cell transcriptomic data across different conditions, technologies, and species. *Nat. Biotechnol.*, **36**(5):411-420. https://dx.doi.org/10.1038/nbt.4096

Christ, A., Gunther, P., Lauterbach, M.A.R.*, et al.*, 2018. Western diet triggers nlrp3-dependent innate immune reprogramming. *Cell*, **172**(1-2):162-175. https://dx.doi.org/10.1016/j.cell.2017.12.013

de Mendonca, E., Fragoso, M.B.T., de Oliveira, J.M.*, et al.*, 2022. Gestational diabetes mellitus: The crosslink among inflammation, nitroxidative stress, intestinal microbiota and alternative therapies. *Antioxidants*, **11**(1):129. https://dx.doi.org/10.3390/antiox11010129

Ding, G.L., Wang, F.F., Shu, J.*, et al.*, 2012. Transgenerational glucose intolerance with igf2/h19 epigenetic alterations in mouse islet induced by intrauterine hyperglycemia. *Diabetes*, **61**(5):1133-1142. https://dx.doi.org/10.2337/db11-1314

Dong, X., Lin, D., Sheng, J.*, et al.*, 2021. Intrauterine hyperglycemia induces liver inflammation in mouse male offspring. *Int. Immunopharmacol.*, **99**:107974. https://dx.doi.org/10.1016/j.intimp.2021.107974

Fang, J., Wu, X., He, J.*, et al.*, 2023. Rbm15 suppresses hepatic insulin sensitivity of offspring of gestational diabetes mellitus mice via m6a-mediated regulation of cldn4. *Mol. Med.*, **29**(1):23. https://dx.doi.org/10.1186/s10020-023-00615-8

Foo, R.X., Ma, J.J., Du, R.*, et al.*, 2024. Gestational diabetes mellitus and development of intergenerational non-alcoholic fatty liver disease (nafld) after delivery: A systematic review and meta-analysis. *EClinicalMedicine*, **72**:102609. https://dx.doi.org/10.1016/j.eclinm.2024.102609

Gao, S., Shi, Q., Zhang, Y.*, et al.*, 2022. Identification of hsc/mpp expansion units in fetal liver by single-cell spatiotemporal transcriptomics. *Cell Res.*, **32**(1):38-53. https://dx.doi.org/10.1038/s41422-021-00540-7

Gong, L., Jiang, S., Tian, J.*, et al.*, 2024. Stz-induced gestational diabetes exposure alters pten/akt/mtor-mediated autophagy signaling pathway leading to increase the risk of neonatal hypoxic-ischemic encephalopathy. *Reprod. Toxicol.*, **123**:108494. https://dx.doi.org/10.1016/j.reprotox.2023.108494

Govindarajah, V., Sakabe, M., Good, S.*, et al.*, 2024. Gestational diabetes in mice induces hematopoietic memory that affects the long-term health of the offspring. *J. Clin. Invest.*, **134**(2):e169730. https://dx.doi.org/10.1172/JCI169730

Hadarits, O., Zoka, A., Barna, G.*, et al.*, 2016. Increased proportion of hematopoietic stem and progenitor cell population in cord blood of neonates born to mothers with gestational diabetes mellitus. *Stem. Cells Dev.*, **25**(1):13-17. https://dx.doi.org/10.1089/scd.2015.0203

Haghverdi, L., Lun, A.T.L., Morgan, M.D.*, et al.*, 2018. Batch effects in single-cell rna-sequencing data are corrected by matching mutual nearest neighbors. *Nat. Biotechnol.*, **36**(5):421-427. https://dx.doi.org/10.1038/nbt.4091

Harris, J.M., Esain, V., Frechette, G.M.*, et al.*, 2013. Glucose metabolism impacts the spatiotemporal onset and magnitude of hsc induction in vivo. *Blood*, **121**(13):2483-2493. https://dx.doi.org/10.1182/blood-2012-12-471201

Jiang, Y., Zhu, H., Chen, Z.*, et al.*, 2022. Hepatic igf2/h19 epigenetic alteration induced glucose intolerance in gestational diabetes mellitus offspring via foxo1 mediation. *Front. Endocrinol.*, **13**:844707. https://dx.doi.org/10.3389/fendo.2022.844707

Lee, R.D., Munro, S.A., Knutson, T.P.*, et al.*, 2021. Single-cell analysis identifies dynamic gene expression networks that govern b cell development and transformation. *Nat. Commun.*, **12**(1):6843. https://dx.doi.org/10.1038/s41467-021-27232-5

Luo, S.S., Zou, K.X., Zhu, H.*, et al.*, 2022. Integrated multi-omics analysis reveals the effect of maternal gestational diabetes on fetal mouse hippocampi. *Front. Cell Dev. Biol.*, **10**:748862. https://dx.doi.org/10.3389/fcell.2022.748862

McGinnis, C.S., Murrow, L.M., Gartner, Z.J., 2019. Doubletfinder: Doublet detection in single-cell rna sequencing data using artificial nearest neighbors. *Cell Syst.*, **8**(4):329-337. https://dx.doi.org/10.1016/j.cels.2019.03.003

McIntyre, H.D., Catalano, P., Zhang, C.*, et al.*, 2019. Gestational diabetes mellitus. *Nat. Rev. Dis. Primers.*, **5**(1):47. https://dx.doi.org/10.1038/s41572-019-0098-8

Miyamoto, Y., Kikuta, J., Matsui, T.*, et al.*, 2024. Periportal macrophages protect against commensal-driven liver inflammation. *Nature*, **629**(8013):901-909. https://dx.doi.org/10.1038/s41586-024-07372-6

Pascoe, C.D., Basu, S., Schwartz, J.*, et al.*, 2022. Maternal diabetes promotes offspring lung dysfunction and inflammation in a sex-dependent manner. *Am. J. Physiol. Lung Cell Mol. Physiol.*, **322**(3):L373-L384. https://dx.doi.org/10.1152/ajplung.00425.2021

Penaloza, H.F., Olonisakin, T.F., Bain, W.G.*, et al.*, 2021. Thrombospondin-1 restricts interleukin-36gamma-mediated neutrophilic inflammation during pseudomonas aeruginosa pulmonary infection. *mBio*, **12**(2):e03336-03320. https://dx.doi.org/10.1128/mBio.03336-20

Pinney, S.E., Joshi, A., Yin, V.*, et al.*, 2020. Exposure to gestational diabetes enriches immune-related pathways in the transcriptome and methylome of human amniocytes. *J. Clin. Endocrinol. Metab.*, **105**(10):3250-3264. https://dx.doi.org/10.1210/clinem/dgaa466

Sun, X., Wu, J., Liu, L.*, et al.*, 2022. Transcriptional switch of hepatocytes initiates macrophage recruitment and t-cell suppression in endotoxemia. *J. Hepatol.*, **77**(2):436-452. https://dx.doi.org/10.1016/j.jhep.2022.02.028

Xie, X., Shi, Q., Wu, P.*, et al.*, 2020. Single-cell transcriptome profiling reveals neutrophil heterogeneity in homeostasis and infection. *Nat. Immunol.*, **21**(9):1119-1133. https://dx.doi.org/10.1038/s41590-020-0736-z

Yan, Y.S., Mo, J.Y., Huang, Y.T.*, et al.*, 2024. Intrauterine hyperglycaemia during late gestation caused mitochondrial dysfunction in skeletal muscle of male offspring through creb/pgc1a signaling. *Nutr. Diabetes*, **14**(1):56. https://dx.doi.org/10.1038/s41387-024-00299-x

Yang, Y., Guo, F., Peng, Y.*, et al.*, 2021. Transcriptomic profiling of human placenta in gestational diabetes mellitus at the single-cell level. *Front. Endocrinol.*, **12**:679582. https://dx.doi.org/10.3389/fendo.2021.679582

Yin, M., Zhang, Y., Li, X.*, et al.*, 2024. Adverse effects of gestational diabetes mellitus on fetal monocytes revealed by single-cell rna sequencing. *iScience*, **27**(1):108637. https://dx.doi.org/10.1016/j.isci.2023.108637

Zakharov, P.N., Hu, H., Wan, X.*, et al.*, 2020. Single-cell rna sequencing of murine islets shows high cellular complexity at all stages of autoimmune diabetes. *J. Exp. Med.*, **217**(6):e20192362. https://dx.doi.org/10.1084/jem.20192362

Zhang, L., Zhang, Y., Wei, L.*, et al.*, 2024. Gestational diabetes mellitus affects the differentiation of hematopoietic stem cells in neonatal umbilical cord blood. *Arch. Gynecol. Obstet*, **310**(2):1109-1119. https://dx.doi.org/10.1007/s00404-024-07513-2

Zhao, Y., Olonisakin, T.F., Xiong, Z.*, et al.*, 2015. Thrombospondin-1 restrains neutrophil granule serine protease function and regulates the innate immune response during klebsiella pneumoniae infection. *Mucosal Immunol.*, **8**(4):896-905. https://dx.doi.org/10.1038/mi.2014.120

Zhong, J., Mao, X., Li, H.*, et al.*, 2022. Single-cell rna sequencing analysis reveals the relationship of bone marrow and osteopenia in stz-induced type 1 diabetic mice. *J. Adv. Res.*, **41**:145-158. https://dx.doi.org/10.1016/j.jare.2022.01.006

Zhu, H., Chen, B., Cheng, Y.*, et al.*, 2019. Insulin therapy for gestational diabetes mellitus does not fully protect offspring from diet-induced metabolic disorders. *Diabetes*, **68**(4):696-708. https://dx.doi.org/10.2337/db18-1151

Zou, K., Ren, J., Luo, S.*, et al.*, 2021. Intrauterine hyperglycemia impairs memory across two generations. *Transl. Psychiatry*, **11**(1):434. https://dx.doi.org/10.1038/s41398-021-01565-7

**Supplementary information**

Table S1; Figs. S1-S7